Vibration-Based Terrain Classification Using Surface Profile Input Frequency Responses

Emmanuel G. Collins, Jr., *Senior Member IEEE*, and Eric J. Coyle

***Abstract*—Terrain variations can greatly influence autonomous ground vehicle (AGV) performance. However, if the terrain is properly identified, the AGV control systems can be adjusted to better suit the terrain. Current terrain classification techniques are largely based on vision and terrain dependent vehicle reactions. But at this time both methods have limitations. Visual methods can easily be fooled by fallen leaves or other superficial ground coverings, whereas response-based methods yield poor results when the AGV speed is significantly different from the training speeds. In addition, current response-based methods are not capable of identifying the multiple terrains that a vehicle may simultaneously traverse, e.g., when one subset of wheels is on-road and one is off-road. This paper proposes a response-based method called *Terrain Input Classification* to solve the issue of speed dependency and multiple terrain traversal. This method is dependent upon knowing the vibration transfer function of the AGV. The method has been verified through terrain-based simulation results and is ready for experimental testing.**

I. Introduction

AUTONOMOUS ground vehicles (AGVs) are expected to operate off-road for search and rescue missions, reconnaissance, agricultural applications, etc. Hence, they will be required to traverse a variety of terrains. Without properly tuning the vehicle control systems to a given terrain, vehicle performance can degrade and can even lead to the vehicle being disabled (e.g., it may get stuck in mud). Specializing the control system to an individual terrain could include enforcing a lower bound on the maximum turning radius, altering the vehicle suspension system or limiting the vehicle speed. An example of a terrain-dependent control system is the Terrain Response system designed for the Land Rover LR3 SUV [1]. The LR3's Terrain Response system has modes for everyday driving, grass/gravel/snow, mud and ruts, sand, and rock crawls. Each mode has predefined settings that change vehicle parameters such as anti-lock braking, throttle response, and differential locking. However, it is up to the LR3's driver to recognize the terrain and switch the system into the proper mode. Since AGVs need to be able to detect terrains without the assistance of a human operator, terrain classification algorithms are essential to any AGV terrain response system.

Current detection methods are largely based on vision or observed vehicle responses. Visual methods, or *sight* detection, rely on processing images created from laser range finders or cameras [2], [3], [4]. In contrast, response-based methods, or *feel* detection, is conducted through sensing internal and external changes, including wheel slip, wheel sinkage, induced sounds, or more commonly, vehicle vibrations [5], [6], [7], [8], [9], [10], [11]. The future of terrain classification will probably rely on both methods, similar to the way a human driver detects terrain changes. However, this paper focuses solely on improving response-based methods.

Recent research in vibration-based terrain classification, which was originally suggested in [12], has proven that vibration signals possess terrain signatures when transformed into the frequency domain [9]. Parallel research has shown improved accuracy by incorporating multiple vibration measurements recorded using an Inertial Measurement Unit (IMU) [7]. The problem with using vehicle responses is that the terrain signatures change when the vehicle is operated at different speeds. This requires training at a large number of speeds within the AGV's operating range, which can be quite large and lead to the need for numerous experiments. Using eigenspace features [6] was able to classify terrains at untrained speeds, but only at slow speeds within a small range (0.5, 5) cm/s. The approach in [10] considers higher speeds in the range (0.6, 1.4) m/s^2, but the tested speeds and training speeds were relatively close together (within 0.2 m/s).

Another limitation of current vibration-based methods is that each wheel is assumed to experience the same terrain [6], [7], [9], [10]. However, situations can occur where vehicle performance could be improved by independently detecting the terrain underneath each wheel. For example, consider an AGV that is attempting to follow a road. If the vehicle slowly veers off the road, the wheels on one side of the robot will experience a new terrain, while the remaining wheels continue on the road surface. If this new terrain causes a large amount of wheel slip, the robot could experience steering difficulties or be forced to slow down. By detecting both the road and new terrain, the vehicle could adjust its steering and drive mechanisms so that the vehicle is fully on the road as desired. The term *multiple terrain traversal* is used in this paper to describe situations in which an AGV simultaneously travels on two or more terrains.

Manuscript submitted February 4, 2008. Prepared through collaborative participation in the Robotics Consortium sponsored by the U.S. Army Research Laboratory under the Collaborative Technology Alliance Program Cooperative Agreement DAAC 19-01-0-0012. The U. S. Government is authorized to reproduce and distribute the reprints for Government purposes notwithstanding any copyright notation thereon.

Emmanuel G. Collins, Jr. and Eric J. Coyle are with the Department of Mechanical Engineering at the FAMU/FSU College of Engineering, Tallahassee, FL 32310 USA USA They are also with the Center for Intelligent Systems, Control and Robotics, Tallahassee, FL 32310 USA (phone: 850-410-6389 and 850-410-6389 email: ecollins and coyleer@eng.fsu.edu).

This paper presents a novel method for vibration-based terrain identification for AGVs called *Terrain Input Classification* (*TIC*). This method addresses the issue of speed dependence as well as multiple terrain traversal. The novelty of this method comes from viewing the vehicle as an open loop system, where the inputs are the surfaces under each wheel and the outputs are the resulting robot vibrations. Instead of performing classification on the vibration outputs as in previous research [6], [7], [8], [9], [10], these outputs and the system vibration transfer function are used to obtain the frequency response of the terrain inputs. Each input is then classified using a Probabilistic Neural Network (PNN), in a manner similar to that in [7], [8]. Although obtaining the system vibration transfer function experimentally is desired for application of this process to a given vehicle, analytical models are used here to verify the approach through simulation.

This paper is composed of four main sections. Section II describes the basic concepts of the proposed TIC approach using a 1 degree-of-freedom (DOF) vibration model, followed by a description of how to implement the approach using a more realistic 3 DOF model. Section III presents simulation results and Section IV gives conclusions.

II. Basic Concepts

Previous research has shown that vibration outputs have specific terrain signatures [7], [8]. *These terrain signatures are the direct result of terrain signatures in the AGV inputs, which are the terrain surfaces.* It will be shown that there is a simple mathematical relationship that can be used to predict the difference in terrain inputs caused by changes in speed. By using this relationship and basing classification on the surface profile inputs, speed independent terrain classification can be performed. That is, in theory it is only necessary to train the classification algorithm at one speed.

In this section the basic concepts of the proposed classification scheme are first presented using the single input-single output (SISO), 1 degree-of-freedom (DOF) model shown in Fig. 1.

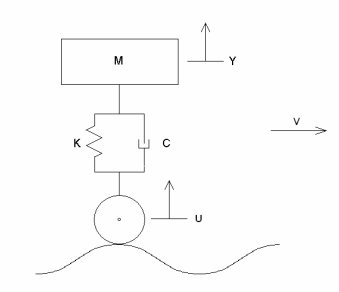

Fig. 1. One Degree of Freedom Model

In particular, this model is used to describe how to obtain the frequency response of the terrain inputs as well as analyze the affects of speed. This discussion leads to a better understanding of why terrain classification based solely on output vibrations is speed dependent. After the initial presentation, this section shows how conclusions drawn from this simplified model, can be applied to a more realistic multi-input multi-output (MIMO) 3 DOF vibration model of an AGV.

A. *Illustration Using a Simplified Model*

The transfer function of Fig. 1 is

$$M(s) = \frac{Y(s)}{U(s)} = \frac{cs+k}{ms^2+cs+k}. \quad (1)$$

Now, assume that the surface along which the system in Fig. 1 is moving is sinusoidal. Also, assume that the system is moving at a constant speed $v = v_1$. Then, input $u(t)$ is a time dependent sinusoid, such that:

$$u(t) = u_1(t) = A\sin(\omega_1 t), \quad (2)$$

If the vehicle now travels the same path at a new speed $v = v_2$, then

$$u(t) = u_2(t) = A\sin(\omega_2 t), \quad (3)$$

where the velocities and frequencies have the relationship,

$$\frac{\omega_1}{\omega_2} = \frac{v_1}{v_2} \overset{\Delta}{=} r. \quad (4)$$

From this simple analysis it is apparent that given an arbitrary surface, the frequency response of the input $u_1(t)$ resulting from traversing the terrain at a velocity $v = v_1$ can be obtained from the frequency response of the input $u_2(t)$ resulting from traversing the same terrain at a velocity $v = v_2$ using

$$U_1(j\omega) = U_2(jr\omega) \quad (5)$$

Hence, suppose $u_1(t)$ and $u_2(t)$ with $r = 0.5$ are generated by a random surface profile and are given by Fig. 2a, and $|U_1(j\omega)|$ and $|U_2(j\omega)|$, shown in Fig. 2b, are the magnitudes of the corresponding frequency responses. If $|U_1(j\omega)|$, obtained at speed v_1 is the terrain signature, then $|U_2(j\omega)|$ obtained at speed v_2, can be mapped to $|U_1(j\omega)|$ using (5).

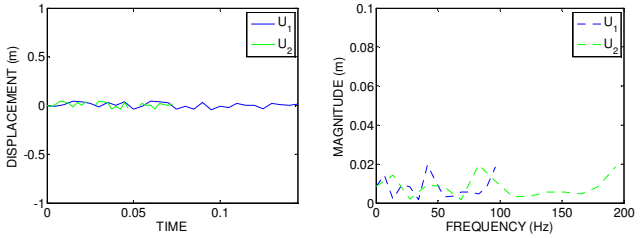

a) time domain b) frequency domain

Fig. 2. Random Terrain Surface

Although directly measuring the terrain input $u(t)$ is extremely difficult using proprioceptive sensors, $U(j\omega)$ can be computed using the recorded output $y(t)$ and the system transfer function. In particular, since

$$Y(j\omega) = M(j\omega)\,U(j\omega) \quad (6)$$

$$U(j\omega) = M(j\omega)^{-1}\, Y(j\omega) \qquad (7)$$

It follows from (6) that $Y_1(j\omega) = M(j\omega)\, U_1(j\omega)$ and $Y_2(j\omega) = M(j\omega)\, U_2(j\omega)$ do *not* have an analogous relationship to (5), i.e.,

$$Y_1(j\omega) \neq Y_2(jr\omega). \qquad (8)$$

In fact, the magnitude and phase changes associated with $M(j\omega)$ *and resulting in (6) make terrain classification based on vibration outputs speed dependent.*

Now assume that in (1), the parameters are given by $m = 1\,(kg)$, $c = 25\,(N\ s/m)$ and $k = 50\,(N/m)$. Also, assume the outputs $y_1(t)$ and $y_2(t)$ corresponding to the inputs $u_1(t)$ and $u_2(t)$ in Fig. 2 are known. Then the input frequency response $U_1(j\omega) = U_2(jr\omega)$ can be computed using the mapping process defined in (7). The magnitudes of the true inputs $U_1(j\omega)$ and $U_2(j\omega)$, and the mapped inputs $\hat{U}_1(j\omega)$ and $\hat{U}_2(jr\omega)$ are shown in Fig. 3. The frequency of inputs $U_2(j\omega)$ and $\hat{U}_2(jr\omega)$ has been scaled using (5)

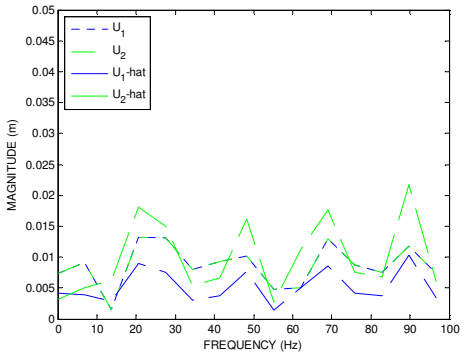

Fig. 3. Magnitudes of the True Fourier Transform $U_1(j\omega)$ and the Mapped Fourier Transforms $\hat{U}_1(j\omega)$ and $\hat{U}_2(jr\omega)$.

From Fig. 3 it is obvious that the mapping process is not perfectly accurate. It seems that the mapped inputs $\hat{U}_1(j\omega)$ and $\hat{U}_2(jr\omega)$ are fairly accurate at frequencies less than 60 Hz, but at higher frequencies the mapping process degrades. This phenomenon is a result of low system magnitude of $M(j\omega)$ at higher frequencies, as shown in Fig. 4.

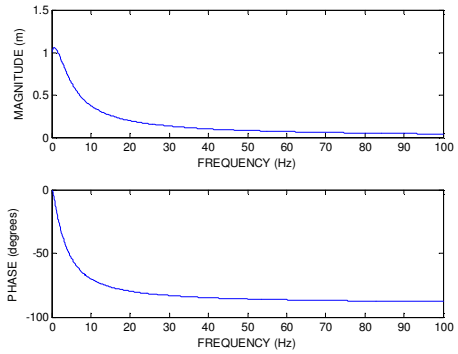

Fig. 4. Bode Plot for G(s) in (8)

In general, if ω is a frequency where $M(j\omega)$ has low magnitude, then the inverse $M^{-1}(j\omega)$ is ill-conditioned, which can introduce substantial errors when $U(j\omega)$ is computed using (7). Since, in this case $M^{-1}(j\omega)$ is large, it will also amplify small errors in $Y(j\omega)$. If instead of using the displacement $y(t)$ as the output, the velocity $\dot{y}(t)$ or the acceleration output $\ddot{y}(t)$ is used, the frequencies that experience low system magnitude will change. In fact, low magnitude would be experienced at lower frequencies, while the higher frequency magnitudes would tend to lead to good conditioning in the inverse transfer function. However, note that for acceleration outputs the transfer function becomes noncausal (since an s^2 is added to the numerator in (1)). Hence, acceleration outputs may not lead to the best classification performance.

The only other difference between the mapped inputs $\hat{U}_1(j\omega)$ and $\hat{U}_2(jr\omega)$ is that the inputs might be known at different frequencies. This is an inherent problem associated with discrete sampling and scaling the frequency range. For example, suppose $r = 1.2$ and the system output is sampled at a rate of $T = 0.01\text{sec}$ for one second. Then the input $\hat{U}_1(j\omega)$ will be defined at every 1.01 Hz from 0 to 100 Hz, but since the frequency range of $\hat{U}_2(jr\omega)$ is scaled based on (4), $\hat{U}_2(jr\omega)$ will be known at every 0.84 Hz from 0 to 83.3 Hz. The frequencies where these two inputs would be known in the range of [0, 10] Hz is shown below in Fig. 5.

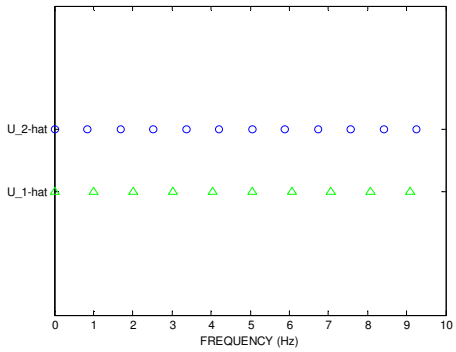

Fig. 5. Example of mismatching frequencies

In practice, inputs defined at relatively the same frequency can be directly compared since the response will be relatively unchanged between those frequencies. For example, the response of one input at 1 Hz might be directly compared to the response of a different input at 1.01 Hz. A qualitative understanding of how close frequencies must be to have approximately the same response will be addressed experimentally in future work. It should be noted that faster sampling rates and longer traversal times will allow comparison of inputs with a larger disparity in speed since the inputs will be defined at more frequencies.

B. *Applications to a 3D Model*

Since as stated with the SISO system, directly measuring the terrain profile with proprioceptive sensors is extremely difficult, a MIMO model will be used to determine the input frequency response. The extension of the results from the SISO 1 DOF system of Fig. 1 to a MIMO multi-DOF system are fairly straightforward if the MIMO system has the same number of inputs and outputs. However, in general this is not the case. For example, consider the 3 DOF, four-input, three-output system shown in Fig. 6. The system inputs are the surface profiles on the 4 wheels, while the system outputs are the vertical velocity, pitch rate and roll rate.

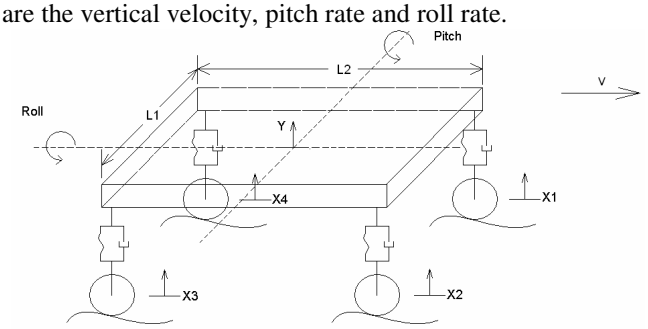

Fig. 6. Vibration Schematic of Four Wheeled Robot with Three Degrees of Freedom

To develop a vibration model for the system using traditional modeling techniques [13], several assumptions were used. First, the frame of this vehicle was treated as a rigid body with a center of mass in the geometric center. Second, the geometry of the tires was ignored and each tire was modeled as the combination of a linear spring and damper. Next, it was assumed that the wheels never lose contact with the ground and the direction of the contact force was assumed to always be in the vertical direction. Next, small angle approximations were used in order to make the model linear. For simplification the robot was assumed to be moving in a straight line at constant speed. This allowed the affects of turning and accelerating or decelerating on the vertical velocity and angular rates to be ignored and ensured that all of the wheels had the same speed. The resulting model is given by

$$Z(s) = G(s)\,X(s) \tag{9}$$

where

$$Z(s) = \begin{bmatrix} \dot{Y}(s) \\ \omega_{pitch}(s) \\ \omega_{roll}(s) \end{bmatrix}, \quad X(s) = \begin{bmatrix} X_1(s) \\ X_2(s) \\ X_3(s) \\ X_4(s) \end{bmatrix}, \tag{10}$$

$$G(s) = \begin{bmatrix} G_1(s) & G_1(s) & G_1(s) & G_1(s) \\ G_2(s) & G_2(s) & -G_2(s) & -G_2(s) \\ G_3(s) & -G_3(s) & -G_3(s) & G_3(s) \end{bmatrix},$$

and

$$G_1(s) = \frac{cs^2 + ks}{ms^2 + 4cs + 4k},$$
$$G_2(s) = \frac{\frac{L_2}{2}cs^2 + \frac{L_2}{2}ks}{I_p s^2 + L_2^2 cs + L_2^2 k}, \tag{11}$$
$$G_3(s) = \frac{\frac{L_1}{2}cs^2 + \frac{L_1}{2}ks}{I_r s^2 + L_1^2 cs + L_1^2 k},$$

where c and k are the damping and spring constant of each tire, I_r is the mass moment of inertia about the roll axis and I_p is the mass moment of inertia about the pitch axis. Based on a scaled car model, appropriate values for the spring and damping constants of the Pioneer 3-AT were chosen [14] and the other parameters in (9) measured directly from the robot. The resulting transfer function matrix $G(s)$ is defined by

$$G_1(s) = \frac{100s^2 + 9000s}{12s^2 + 400s + 3600},$$
$$G_2(s) = \frac{14s^2 + 1260s}{0.12s^2 + 7.84s + 704.6}, \tag{12}$$
$$G_3(s) = \frac{20s^2 + 1800s}{0.2s^2 + 16s + 1440}.$$

The terrain profiles were extracted from real terrains using the Laser Line Striper developed at the Carnegie Melon University Robotics Institute [15]. This device uses triangulation based on a camera and laser, as shown in Fig. 7, to determine the inertial coordinates of each laser point. Fig. 8 shows example images and profiles for sand and grass.

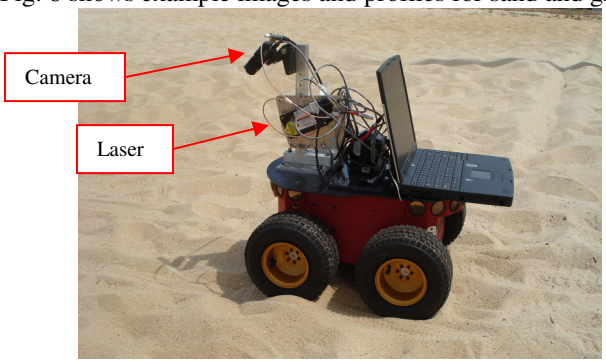

Fig. 7. Pioneer 3-AT Robot Platform, the Laser Line Striper Consists of the Camera and Laser components as Labeled

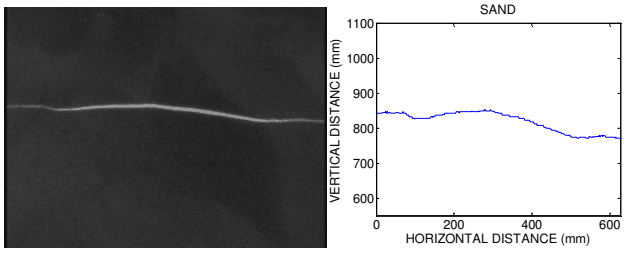

a) Sand

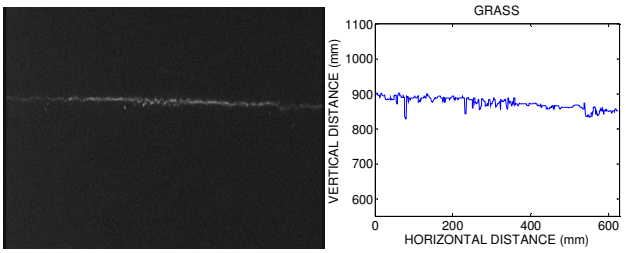

b) Grass

Fig. 8. Example Laser Line Striper Images and Plots

Although real terrains will deform when the robot drives over them, these profiles were treated as hard surfaces in the simulations. From these spatial profiles, time-varying input signals were created by assuming a traversal speed. This allows the time-varying outputs $\dot{y}(t)$, $\omega_{roll}(t)$ and $\omega_{pitch}(t)$ to be simulated using (9), (10) and (12). The frequency response $Z(j\omega)$ of the simulated outputs is then obtained using a Fast Fourier Transform (FFT). Equation (9) then yields that $X(j\omega)$ is a solution to

$$Z(j\omega) = G(j\omega)\, X(j\omega). \qquad (13)$$

Equation (13) has a unique solution if the number of inputs and outputs is equal. Under the ideal situation in which $G(s)$ exactly represents the real system, the measurements are perfect and noiseless and the assumption that the surface is perfectly rigid is true, then if there are more outputs than inputs, (13) is a consistent equation and it has a unique solution. However, since these ideal conditions are never met, the least squares solution may suffice. If the number of outputs is less than the number of inputs, which is the case considered here, then there are in general an infinite number of solutions and some means must be sought for finding one meaningful solution, a key problem in TIC.

One solution to (13) is the least squares solution. But since this is an under-determined system of equations, there are an infinite number of least squares solutions. One least squares solution often used in under-determined systems is the minimal least squares solution, calculated using the Moore-Penrose inverse. This least squares solution minimizes both the squared error and the norm of the computed inputs. However, it was found here that minimal least squares solutions typically result in calculated inputs of nearly the same magnitude. When all four wheels, and thus all four inputs, are of the same terrain this is an advantageous property as shown in Fig. 9a since terrain signatures are expected to have nearly the same magnitude. In this figure it can be seen that when the input to the left side wheels is a sand profile X_a and the input to the right side wheels is a different sand input X_b, then the computed inputs $\hat{X}_a$ and $\hat{X}_b$ look extremely similar, which is advantageous for classification. But, during multiple terrain traversal, minimal least squares solutions make the terrain of each input difficult to determine. This can be seen in Fig. 9b where a sand profile X_a is the input to the left side wheels, and a grass profile X_b is the input to the right side wheels. Fig. 9b shows an increase in magnitude for the computed sand profile $\hat{X}_a$ compared to Fig. 9a. Additionally, the computed inputs $\hat{X}_a$ and $\hat{X}_b$ in Fig. 9a are extremely similar, which will make inputs of different terrains extremely difficult to classify. Thus a different method of finding a solution to (13) was sought with the purpose of detecting multiple terrain traversal while maintaining speed independence.

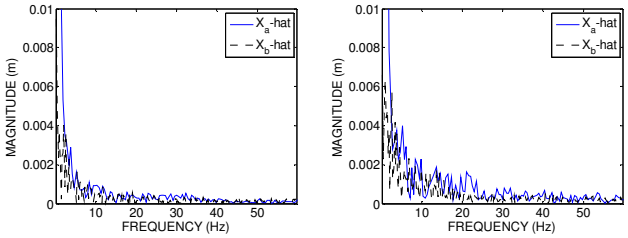

a) All inputs are Sand Terrain b) Sand paired with Grass

Fig. 9. Example Minimal Least Squares Solutions

Since inputs from the same terrain are expected to have approximately the same magnitude frequency response, nonlinear constraints could be used to find a more appropriate solution to (13). Since the front wheels are close in proximity to the back wheels, the front and back wheels on the same side of the AGV will typically experience the same terrain. Thus in the four input, three output case in Fig. 6 inputs X_1 and X_4 are expected to be from the same terrain and inputs X_2 and X_3 are expected to be from the same terrain. The resulting nonlinearly constrained optimization problem then becomes

$$\min_{X(j\omega)} [Z(j\omega) - G(j\omega)X(j\omega)]^T [Z(j\omega) - G(j\omega)X(j\omega)] \qquad (14)$$

subject to

$$|X_1(j\omega)| = |X_4(j\omega)|,\ |X_2(j\omega)| = |X_3(j\omega)|. \qquad (15)$$

Although the optimization problem (14)-(15) will be considered in future research, below less computationally intensive alternatives are presented which make assumptions on the difference in phase between specified input pairs, $\{X_1(j\omega), X_4(j\omega)\}$ and $\{X_2(j\omega), X_3(j\omega)\}$.

When the AGV is moving in a straight line, assuming a rigid surface, the inputs to the back wheels will be the same input seen by the corresponding front wheels with a difference in phase caused by a time delay. This leads to the constraint equations $X_4(j\omega) = X_1(j\omega)\, e^{-jw\tau}$ and $X_3(j\omega) = X_2(j\omega)\, e^{-jw\tau}$, where τ is the time delay in seconds. The above constraints along with (9), (10), and (11) yields

$$\begin{bmatrix} X_1(j\omega) \\ X_2(j\omega) \end{bmatrix} = \begin{bmatrix} G_1(j\omega)(1+e^{-j\omega\tau}) & G_1(j\omega)(1+e^{-j\omega\tau}) \\ G_3(j\omega)(1+e^{-j\omega\tau}) & -G_3(j\omega)(1+e^{-j\omega\tau}) \end{bmatrix}^{-1} \begin{bmatrix} \dot{Y}(j\omega) \\ \omega_{roll}(j\omega) \end{bmatrix}. \qquad (16)$$

Unfortunately, the elements of the transfer function matrix in (16) periodically become zero as a result of model symmetry, as illustrated in Fig. 10. At the frequencies where

these elements are zero, the matrix is singular, which leads to an ill-conditioned inverse problem. This method also assumes that the front wheels do not deform the surface, which can be a poor assumption for some surface types. Hence, another mechanism for finding a suitable solution $X(j\omega)$ must be sought.

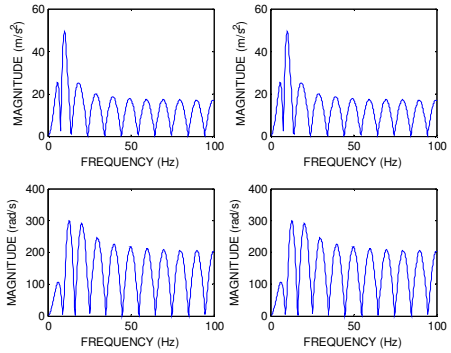

Fig. 10. System Frequency Response Magnitudes using the Delay Reduction Method

Now, assume the nonlinear constraints of (15) are approximated by $X_4(j\omega) = X_1(j\omega)$ and $X_3(j\omega) = X_2(j\omega)$. Then (13) yields,

$$\begin{bmatrix} \hat{X}_1(j\omega) \\ \hat{X}_2(j\omega) \end{bmatrix} = \begin{bmatrix} 2G_1(j\omega) & 2G_1(j\omega) \\ 2G_3(j\omega) & -2G_3(j\omega) \end{bmatrix}^{-1} \begin{bmatrix} \dot{Y}(j\omega) \\ \omega_{roll}(j\omega) \end{bmatrix}. \quad (17)$$

Imagine an AGV that has two wheels, one on the right and one on the left, and nearly the same geometry and mass as the original four-wheeled vehicle. Solving by (17) is analogous to trusting that this two-wheeled AGV would experience a roll rate and vertical velocity that is of similar frequency response to that of the four-wheeled vehicle. Any $\hat{X}(j\omega)$ calculated using (17) will be referred to as a *virtual input* since it is an estimate of the true terrain inputs.

Example virtual inputs created from sand and grass profiles are given in Fig. 11. Notice that the virtual inputs in Fig. 11 have distinctly different signatures.

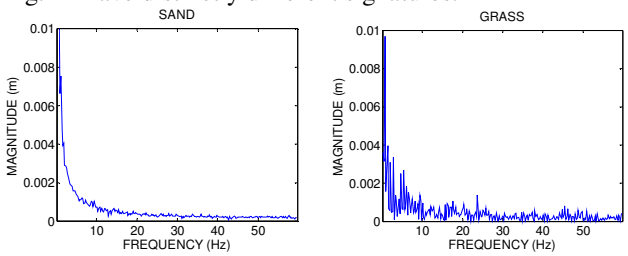

Fig. 11. Examples of Virtual Inputs

Next, consider two virtual inputs of the same terrain with a speed ratio of *r=3* (0.1 m/s and 0.3 m/s). Fig. 12 displays the magnitude of these virtual inputs after altering the frequency scale of the higher speed based on (4). Since the terrain signatures are still evident in Fig. 12 speed independent terrain classification should be possible with this set of virtual inputs. It should be mentioned that in general, if the robot is turning, each wheel will have a different velocity.

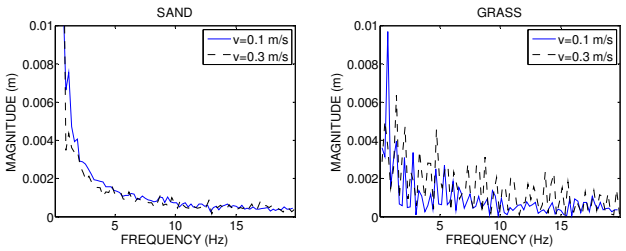

Fig. 12. Examples of Virtual Inputs at Different Speeds

If the velocity of each wheel can be found, e.g., using rigid body dynamics or independent sensor measurements, the left and right side inputs could be computed using different speed ratios. In the next section the virtual inputs are used for classification in TIC.

III. Simulation and Classification Results

Since at this time an experimental set-up to implement TIC is unavailable, simulation results are used to prove its effectiveness. The simulation considered four terrains: sand, grass, gravel and asphalt. Using the Laser Line Striper, 60 surface profiles of approximately 0.8 m in length were obtained for each terrain. These profiles were then separated into training and test sets with twenty profiles per terrain in the test set. Then using the vibration model corresponding to the Pioneer 3 (see (9), (10), and (12)) the output frequency response $Z(j\omega)$ was obtained for the robot moving at constant speeds from 0.1 m/s to 1 m/s at intervals of every 0.1 m/s. Subsequently using (17), test and training virtual inputs were found for each speed.

A PNN was used to classify the virtual inputs based on the frequency response magnitudes. Using the virtual inputs at a specified training speed, this PNN creates a probability density function (pdf) for each terrain. These pdfs are then used to find the probability of a test input belonging to each terrain. The test input is then said to belong to the class with the highest associated probability [16].

It should be noted that using a spatial FFT and PNN only 91.25% of the sample test signals were found to have a terrain signature. Clarification of this method can be found in [17]. To correct for this, the *weighted accuracy* will be used to validate the results. The weighted accuracy is computed using

$$weighted\ accuracy = \frac{overall\ accuracy}{0.9125} \quad (18)$$

This means that an overall classification accuracy of 91.25% will correspond to a weighted accuracy of 100%.

Simulation results found using virtual inputs at the same speed are shown in TABLE 1. Testing and training at the same speed was found to be highly accurate, with a weighted accuracy of almost 96%. Additionally, each terrain was classified with an overall accuracy of at least 80%. However, experimental results may show improved results since terrains such as sand and gravel will violate the hard surface assumption. This means that although the spatial profile of some terrains may be similar, AGV vibrations

could be significantly different on these terrains.

TABLE 1: CLASSIFICATION RESULTS FOR TRAINING AND TESTING AT THE SAME SPEED

		Detected Terrain			
		sand	grass	gravel	asphalt
Tested Terrain	sand	85%		5%	
	grass	5%	85%	10%	
	gravel	10%		80%	10%
	asphalt				100%
		Overall:	87.50%	Weighted:	95.89%

Now, consider the results shown in Fig. 13, which correspond to classifying virtual inputs at untrained speeds. Speed ratios above 1 correspond to testing at a speed of 0.1 m/s and training the PNN at faster speeds. Speed ratios below 1 correspond to training at a speed of 0.1 m/s and testing at faster speeds. This was done to avoid changing the sampling rate, which causes mismatching frequency information, or having to interpolate between points on the surface profile. Instead the outputs at a speed n times faster than another speed is found by using every n^{th} data point in the spatial profile.

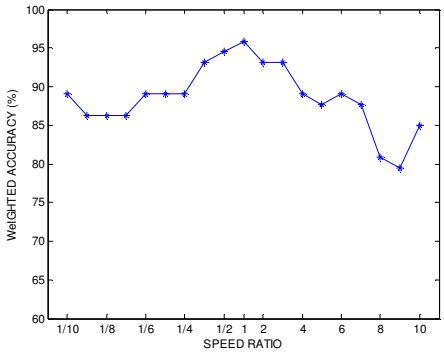

Fig. 13. Classification Accuracy When Training at Different Speeds

Although, discrete sampling does limit the disparity of speeds that can be compared, Fig. 13 shows that vibration input terrain classification is speed independent over a fairly large range. Speed ratios between 1/10 and 7 all resulted in a weighted accuracy of 85% or better. This disparity in speeds is considerably larger than that of previous vibration-based methods [6], [10]. From Fig. 13 it is hard to determine whether training at a faster speed or slower speed is more desirable, as the plot is somewhat symmetric. In fact, there is a natural trade-off between training at faster speeds and training at slower speeds. At faster speeds the AGV will cover a larger length of the terrain. Covering more terrain will reduce the influence of any anomalies in the surface, and make the terrain signature more evident in each trial. However, training at slower speeds has the advantage of taking more samples over the same length of ground. This means that surface details that cannot be seen at faster speeds due to discrete sampling may become evident at slower speeds. Ultimately how much detail is recorded in the vibration outputs will be dependent on the sampling rate and precision of the vibration sensors. For this reason it is difficult to determine the speed where this trade-off will occur without experimental results.

In addition to speed dependence, this algorithm should be able to detect cases where an AGV experiences multiple terrain traversal. To test this theory in simulation, the inputs X_1 and X_4 were allowed to be a different terrain than X_2 and X_3. This enables the terrain on the right side wheels of the AGV to be different from the terrain experienced by the left side wheels. Every combination of terrains using sand, grass, gravel and asphalt was considered. The results of this test are compared to the results without multiple terrain traversal in Fig. 14, which shows that the weighted accuracy was essentially unaffected by multiple terrain traversal. In fact, the weighted accuracy did not change by more than 3% at any of the speed ratios that were considered. This shows that TIC can detect multiple terrain traversal.

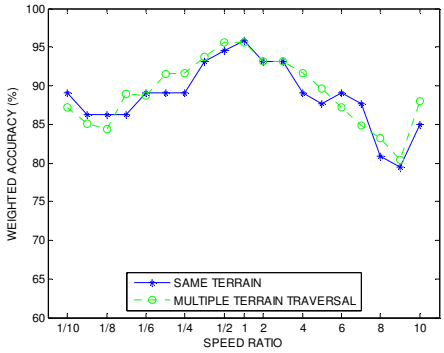

Fig. 14. Weighted Accuracy with Multiple Terrain Traversal

So far it has been shown that TIC can be used to address two of the biggest problems with current vibration-based terrain classification: speed dependence and multiple terrain traversal. However, sensor and model inaccuracies are likely to occur. Errors relating to sensor readings, such as noise or bias, may require filtering or post-processing techniques to improve robustness. The appropriate measures to handle sensor errors will be investigated during the experimental validation process of TIC. Additionally, a vibration model that exactly represents the vibration dynamics of the system will never be available. Inaccuracies in this model can occur due to non-linearity, changes in the dynamics of the system or external influences. Hence, the influence of model error on the simulation results was investigated as well. In particular, the model was allowed to experience a random error in magnitude and phase at each frequency. The affects of a maximum error of 0% to 40% are shown in Fig. 15. Model errors between 0% and 15% were found to have only minimal affects on the simulation results. But as expected a large amount of error, such as 40%, can make classification extremely difficult. Hence, moderate uncertainty can be

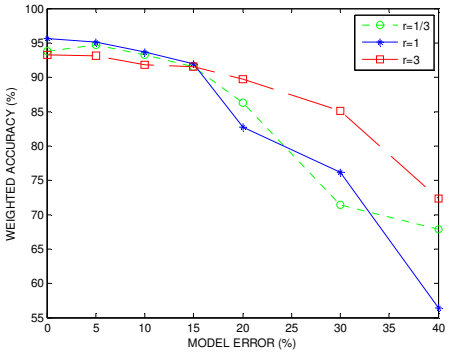

Fig. 15. Classification Results for Multiple Terrain Traversal in the Presence of Model Error

tolerated in the model $G(s)$. An analytically derived model may not have sufficient fidelity. Therefore, it currently seems best to obtain this transfer function via system identification experiments.

One thing that was not addressed in this research is the expected or anticipated update rate of this terrain classification algorithm. It is expected that since terrain classification has been conducted accurately at update rates of once per second at 2 m/s [18], that TIC classification at equal speeds will be possible at a similar rate. However, due to the frequency scaling procedure it will likely require a slower update rate to classify terrains using TIC when the vehicle speed differs from the trained speed. Application of a sliding horizon on classification may reduce the need for slower update rates. Ultimately, an appropriate update rate will be determined when TIC can be implemented experimentally.

IV. Conclusion

In this paper a new vibration-based terrain classification method, Terrain Input Classification, has been presented which improves upon current vibration-based techniques for AGVs by eliminating or reducing speed dependency and by detecting multiple terrain traversal. This method, which maps vibration outputs to the terrain inputs using the AGV vibration transfer function, was verified in simulation using surface profiles from real terrains. Current work is focused on using system identification to obtain this transfer function for an AGV and experimentally implementing TIC. This implementation will likely use several strategic training speeds to accommodate the entire operating range of any AGV, since at extremely fast speeds the robot may loose contact with the ground, which could change the terrain signatures. Future versions of this algorithm may be improved by incorporating knowledge of the environment or by characterizing the likelihood of transitioning between specific terrains. Future research will also consider other methods for approximating terrain inputs such as optimization with nonlinear constraints.

Acknowledgement

The authors would like to thank Martial Herbert and Christoph Mertz at the Carnegie Melon University Robotics Institute for developing and providing the Laser Line Striper which was used to obtain the terrain profiles in these simulations.

References

[1] D. Vanderwerp, 2005. "What does terrain response do?" http://www.caranddriver.com/features/9026/what-does-terrain-response-do.html, July 31, 2007.

[2] M. Hebert, N. Vandapel, S. Keller, R. Rao Donamukkala, "Evaluation and comparison of terrain classification techniques from ladar data for autonomous navigation," *23rd Army Science Conf.*, December 2002.

[3] N. Vandapel, M. Hebert, D. Huber and A. Akapuria, "Natural terrain classification using 3-D ladar data," *IEEE Int. Conf. on Robotics and Automation*, New Orleans, LA, April 2004,.

[4] D. F. Wolf, G. S. Sukhatme, D. Fox, and W. Burgard, "Autonomous terrain mapping and classification using hidden markov models," in *Proc. of IEEE Int. Conf. on Robotics and Automation*, 2005.

[5] K. Iagnemma, C. Brooks, and S. Dubowsky, "Visual, tactile, and vibration-based terrain analysis for planetary rovers," in *Proc. of the 2004 IEEE Aerospace Conf.*, 2004.

[6] C. Brooks, K. Iagnemma, and S. Dubowsky, "Vibration-based terrain analysis for mobile robots," *IEEE Trans. Of Robotics*, vol. 21, no.6 2005, pp. 1185-1191.

[7] E. M. DuPont, C. A. Moore, R. G. Roberts, and E. G. Collins, Jr, "Terrain classification using probabilistic neural networks," in *Proc. of the Florida Conf. on Recent Advances of Robotics*, May 2005.

[8] E. M. DuPont, R. G. Roberts, C. A. Moore, M. F. Selekwa, and E. G. Collins, "Online terrain classification for mobile robots," in *Proc. of IMECE 2005 ASME 2005 Int. Mechanical Engineering Congress and Exposition Conf.*, November 5-11, 2005, Orlando, USA.

[9] L. Ojeda, J. Borenstein, G. Witus, and R. Karlson, "Terrain characterization and classification with a mobile robot," *J. of Field Robotics,* vol. 23 no.3 pp. 103-122, 2006.

[10] E. M. DuPont, R. G. Roberts and C. A. Moore, "The identification of terrains for mobile robots using eigenspace and neural network methods," in *CD Proc. 2006 Florida Conf. on Recent Advances in Robotics*, Miami, Florida, May 25-26, 2006.

[11] A. Angelova, L. Matthies, D. Helmick, G. Sibley, and P. Perona, "Learning to predict slip for ground robots," *IEEE Int. Conf. on Robotics and Automation*, Orlando, Florida, May 15-19, 2006

[12] K. D. Iagnemma and S. Dubowsky, "Terrain estimation for high speed rough terrain autonomous vehicle navigation," in *Proc. SPIE Conf. Unmanned Ground Vehicle Technology IV*, Orlando, FL, 2002

[13] H. Baruh, *Analytical Dynamics*, McGraw-Hill Companies Inc, 1999 p. 215-264.

[14] J.Y. Wong, *Theory of Ground Vehicles*, Third Edition John Wiley & Sons, New York, NY 2001 p. 436-450.

[15] C. Mertz, J. Kozar, J.R. Miller and C. Thorpe, "Eye-safe laser line striper for outside use," *IEEE Intelligent Vehicle symposium,* June 2002, December 2001.

[16] D.F Specht, "Probabilistic neural networks," *Neural Networks,*Vol. 3, No. 1, January 1990, pp. 109-118.

[17] L. Lu, C. Ordonez, E. G. Collins Jr. and E. DuPont, "Terrain identification for autonomous ground vehicles using 2D structured light sensors," *IEEE Int. Conf. on Intelligent Robots and Systems,* submitted for publication.

[18] E. Coyle, E. G. Collins Jr., E. DuPont, D. Ding, H. Wang, R. Cooper and G. Grindle, "Vibration-based terrain classification for electric powered wheelchairs," *IASTED Conf. on Assistive Technologies,* April 2008, submitted for publication.